Noise and Inertia-Induced Inhomogeneity in the Distribution of Small Particles in Fluid Flows

Julyan H. E. Cartwright,[1, *] Marcelo O. Magnasco,[2, †] and Oreste Piro[3, ‡]

[1]*Laboratorio de Estudios Cristalográficos, CSIC, E-18071 Granada, Spain*
[2]*Mathematical Physics Laboratory, The Rockefeller University, Box 212, 1230 York Avenue, NY 10021*
[3]*Institut Mediterrani d'Estudis Avançats, CSIC–UIB, E-07071 Palma de Mallorca, Spain*
(Dated: version of February 8, 2008)

The dynamics of small spherical neutrally buoyant particulate impurities immersed in a two-dimensional fluid flow are known to lead to particle accumulation in the regions of the flow in which rotation dominates over shear, provided that the Stokes number of the particles is sufficiently small. If the flow is viewed as a Hamiltonian dynamical system, it can be seen that the accumulations occur in the nonchaotic parts of the phase space: the Kolmogorov–Arnold–Moser tori. This has suggested a generalization of these dynamics to Hamiltonian maps, dubbed a bailout embedding. In this paper we use a bailout embedding of the standard map to mimic the dynamics of impurities subject not only to drag but also to fluctuating forces modelled as white noise. We find that the generation of inhomogeneities associated with the separation of particle from fluid trajectories is enhanced by the presence of noise, so that they appear in much broader ranges of the Stokes number than those allowing spontaneous separation.

PACS numbers: 47.52.+j, 05.45.Gg, 45.20.Jj

I. INTRODUCTION

Impurities suspended in a fluid flow are frequently observed to be distributed inhomogeneously. Even in very chaotic flows, particulate impurities arrange themselves in extraordinarily structured distributions, in apparent contradiction to the high mixing efficiency expected from the characteristics of the basic flow. To give just one example, in the particular instance of geophysical fluids, the filamentary structure, or patchiness, often displayed by plankton populations in the oceans is a puzzling problem currently under intense investigation [1, 2, 3]. Several mechanisms to produce this type of inhomogeneity have been studied, and include both dynamical aspects of the flow as well as the reactive properties of the considered impurities. The basic idea in these mechanisms is that the particle loss due either to the flow — in open flows — or to the chemical or population dynamics of the particles — in closed flows — is minimized on some manifolds associated with the hyperbolic character of the flow [4, 5, 6]. In this paper we explore an alternative purely dynamical mechanism for inhomogeneity with non-reactive particles in bounded flows. We show that particle inertial effects combined with fluctuating forces are capable of producing inhomogeneity even in cases in which the impurity and fluid densities match exactly.

When impurities have a different density to the fluid, it is intuitively clear that they will be expelled from rapidly rotating regions of the flow — for heavy particles — or attracted to the center of those regions — for light particles — because of centrifugal effects [7]. However, it was recently demonstrated that neutrally buoyant particles also tend to settle in the rotation-dominated regions of a flow, but because of a more subtle mechanism involving the separation between the fluid and particle trajectories that can occur in the opposite regions, i.e., in the areas of the flow dominated by shear [8]. However, this mechanism is only relevant when the particle Stokes number is smaller than the eigenvalues of the Jacobian matrix of the flow, a condition that may not be fulfilled in some physically interesting situations. We show here by means of a minimal model that the latter condition may be relaxed if a small amount of noise be added to the forces acting on the impurity.

Our approach is qualitative, in the sense that instead of considering a specific flow and the precise particle dynamics induced by it, we describe the system with an iterative map whose evolution contains the basic features of both the fluid flow and the particle dynamics: flow volume preservation, together with particle separation at the hyperbolic regions. The reason for moving to a discrete system is that in the map the phenomena that we describe may be understood more intuitively, while translating the results back to the flow case is immediate. The strategy of understanding fluid-dynamical phenomena by using iterated maps amenable to the powerful artillery of dynamical-systems theory has been successfully applied on several different occasions. For example, the structures of the chaotic advection induced by time-periodic three-dimensional incompressible flows were predicted by studying the qualitatively equivalent dynamics of three-dimensional volume-preserving maps [9, 10]. Later, these structures were confirmed in realistic flows [11, 12, 13]. Other examples are the treatment of the propagation of combustion fronts in laminar flows by a qualitative map approach [14], and the description of the formation of plankton population structures due to inhomogeneities of the nutrient sources [15]. Remarkably, in the instance we discuss in this paper, the procedure is also useful from the point of view of dynamical-systems theory, as it has suggested a new technique — bailout embedding — for the control of Hamiltonian chaos [16].

The plan of the paper is as follows. First, we briefly review

*URL: http://lec.ugr.es/~julyan; Electronic address: julyan@lec.ugr.es
†URL: http://asterion.rockefeller.edu/marcelo/marcelo.html; Electronic address: marcelo@sur.rockefeller.edu
‡URL: http://www.imedea.uib.es/~piro; Electronic address: piro@imedea.uib.es

the classical model for the forces acting on a small spherical tracer moving relative to the fluid in which it is immersed (Section II). Concentrating on the case of a neutrally buoyant impurity, we trace the construction of a minimal model that makes evident the separation of particle and fluid trajectories in the regions in which the flow presents strong shear (Section III). On the basis of this model, we make a generalization that allows us to build a discrete mapping that represents the Lagrangian evolution of the fluid parcels as well as the dynamics of the particle (Section IV). While this map also displays particle–fluid separation when the parameter γ, equivalent to the Stokes number, is relatively small, we show in Section V that a small amount of noise, added to the dynamics of the particle to separate it continually from the flow, enhances the impact of the hyperbolic regions far beyond the values of γ required for separation. Conclusions are to be found in Section VI.

II. MAXEY–RILEY EQUATIONS

The equation of motion for a small, spherical tracer in an incompressible fluid we term the Maxey–Riley equation [8, 17, 18], which may be written as

$$
\rho_p \frac{d\boldsymbol{v}}{dt} = \rho_f \frac{D\boldsymbol{u}}{Dt} + (\rho_p - \rho_f)\boldsymbol{g} \tag{1}
$$
$$
- \frac{9\nu\rho_f}{2a^2}\left(\boldsymbol{v} - \boldsymbol{u} - \frac{a^2}{6}\nabla^2\boldsymbol{u}\right)
$$
$$
- \frac{\rho_f}{2}\left(\frac{d\boldsymbol{v}}{dt} - \frac{D}{Dt}\left[\boldsymbol{u} + \frac{a^2}{10}\nabla^2\boldsymbol{u}\right]\right)
$$
$$
- \frac{9\rho_f}{2a}\sqrt{\frac{\nu}{\pi}}\int_0^t \frac{1}{\sqrt{t-\zeta}}\frac{d}{d\zeta}\left(\boldsymbol{v} - \boldsymbol{u} - \frac{a^2}{6}\nabla^2\boldsymbol{u}\right)d\zeta.
$$

Here $\boldsymbol{v}$ represents the velocity of the particle, $\boldsymbol{u}$ that of the fluid, ρ_p the density of the particle, ρ_f, the density of the fluid it displaces, ν, the kinematic viscosity of the fluid, a, the radius of the particle, and $\mathbf{g}$, gravity. The derivative $D\boldsymbol{u}/Dt$ is along the path of a fluid element

$$
\frac{D\boldsymbol{u}}{Dt} = \frac{\partial \boldsymbol{u}}{\partial t} + (\boldsymbol{u}\cdot\boldsymbol{\nabla})\boldsymbol{u}, \tag{2}
$$

whereas the derivative $d\boldsymbol{u}/dt$ is taken along the trajectory of the particle

$$
\frac{d\boldsymbol{u}}{dt} = \frac{\partial \boldsymbol{u}}{\partial t} + (\boldsymbol{v}\cdot\boldsymbol{\nabla})\boldsymbol{u}. \tag{3}
$$

The terms on the right of Eq. (1) represent respectively the force exerted by the undisturbed flow on the particle, buoyancy, Stokes drag, the added mass due to the boundary layer of fluid moving with the particle [19, 20], and the Basset–Boussinesq force [21, 22] that depends on the history of the relative accelerations of particle and fluid. The terms in $a^2\nabla^2\boldsymbol{u}$ are the Faxén [23] corrections. The Maxey–Riley equation is derived under the assumptions that the particle radius and its Reynolds number are small, as are the velocity gradients around the particle.

III. MINIMAL MODEL

First let us consider a minimal model for a neutrally buoyant particle. For this we set $\rho_p = \rho_f$ in Eq. (1). We consider the Faxén corrections and the Basset–Boussinesq term to be negligible. We now rescale space, time, and velocity by scale factors L, $T = L/U$, and U, to arrive at the expression

$$
\frac{d\boldsymbol{v}}{dt} = \frac{D\boldsymbol{u}}{Dt} - \mathrm{St}^{-1}\left(\boldsymbol{v} - \boldsymbol{u}\right) - \frac{1}{2}\left(\frac{d\boldsymbol{v}}{dt} - \frac{D\boldsymbol{u}}{Dt}\right), \tag{4}
$$

where St is the particle Stokes number $\mathrm{St} = 2a^2U/(9\nu L) = 2/9\,(a/L)^2\mathrm{Re}_f$, Re_f being the fluid Reynolds number. The assumptions involved in deriving Eq. (1) require that $\mathrm{St} \ll 1$ in Eq. (4).

If we substitute the expressions for the derivatives in Eqs. (2) and (3) into Eq. (4), we obtain

$$
\frac{d}{dt}\left(\boldsymbol{v} - \boldsymbol{u}\right) = -\left((\boldsymbol{v} - \boldsymbol{u})\cdot\boldsymbol{\nabla}\right)\boldsymbol{u} - \frac{2}{3}\mathrm{St}^{-1}\left(\boldsymbol{v} - \boldsymbol{u}\right). \tag{5}
$$

We may then write $\boldsymbol{A} = \boldsymbol{v} - \boldsymbol{u}$, whence

$$
\frac{d\boldsymbol{A}}{dt} = -\left(J + \frac{2}{3}\mathrm{St}^{-1}\mathrm{I}\right)\cdot\boldsymbol{A}, \tag{6}
$$

where J is the Jacobian matrix — we now concentrate on two-dimensional flows $\boldsymbol{u} = (u_x, u_y)$ —

$$
J = \begin{pmatrix} \partial_x u_x & \partial_y u_x \\ \partial_x u_y & \partial_y u_y \end{pmatrix}. \tag{7}
$$

If we diagonalize the matrix we obtain

$$
\frac{d\boldsymbol{A}_D}{dt} = \begin{pmatrix} \lambda - 2/3\,\mathrm{St}^{-1} & 0 \\ 0 & -\lambda - 2/3\,\mathrm{St}^{-1} \end{pmatrix}\cdot\boldsymbol{A}_D, \tag{8}
$$

so if $Re(\lambda) > 2/3\,\mathrm{St}^{-1}$, $\boldsymbol{A}_D$ may grow exponentially. Now λ satisfies $\det(J - \lambda\mathrm{I}) = 0$, so $\lambda^2 - \mathrm{tr}J + \det J = 0$. Since the flow is incompressible, $\partial_x u_x + \partial_y u_y = \mathrm{tr}J = 0$, thence $-\lambda^2 = \det J$. Given squared vorticity $\omega^2 = (\partial_x u_y - \partial_y u_x)^2$, and squared strain $s^2 = s_1^2 + s_2^2$, where the normal component is $s_1 = \partial_x u_x - \partial_y u_y$ and the shear component is $s_2 = \partial_y u_x + \partial_x u_y$, we may write

$$
Q = \lambda^2 = -\det J = (s^2 - \omega^2)/4, \tag{9}
$$

where Q is the Okubo–Weiss parameter [24, 25]. If $Q > 0$, $\lambda^2 > 0$, and λ is real, so deformation dominates, as around hyperbolic points, whereas if $Q < 0$, $\lambda^2 < 0$, and λ is complex, so rotation dominates, as near elliptic points. Equation (6) together with $d\boldsymbol{x}/dt = \boldsymbol{A} + \boldsymbol{u}$ defines a dissipative dynamical system

$$
d\boldsymbol{\xi}/dt = \boldsymbol{F}(\boldsymbol{\xi}) \tag{10}
$$

with constant divergence $\boldsymbol{\nabla}\cdot\boldsymbol{F} = -4/3\,\mathrm{St}^{-1}$ in the four dimensional phase space $\boldsymbol{\xi} = (x, y, A_x, A_y)$, so that while small values of St allow for large values of the divergence, large values of St force the divergence to be small. The Stokes number

is the relaxation time of the particle back onto the fluid trajectories compared to the time scale of the flow — with larger St, the particle has more independence from the fluid flow. From Eq. (8), about areas of the flow near to hyperbolic stagnation points with $Q > 4/9\,\mathrm{St}^{-2}$, particle and flow trajectories separate exponentially.
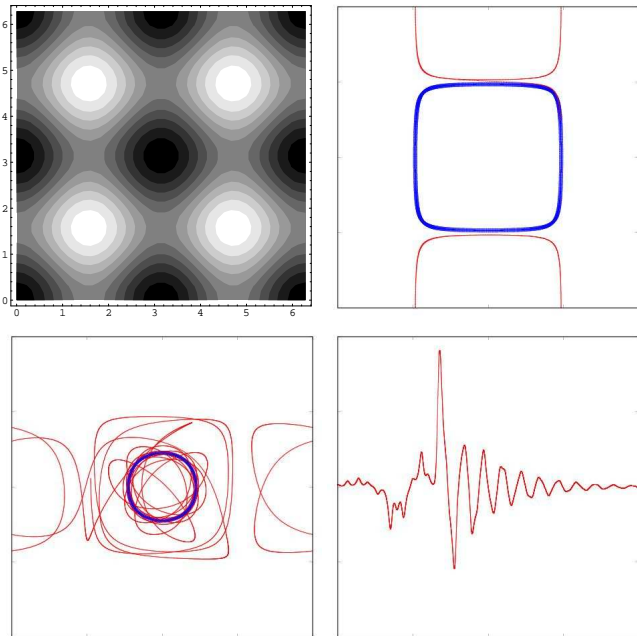

FIG. 1: (a) Contour plot illustrating magnitude of Q — lighter is higher Q — for the time-independent model Eq. (11) (the flow is on a torus). (b) The separation of a neutrally buoyant particle trajectory (red line) from the flow (blue line) in regions of high Q allows the particle to wander between cells. (c) After a complicated excursion, a particle (red line) eventually settles in a zone of low Q of the flow (blue line). (d) The velocity difference $v_x - u_x$ between the particle and the flow against time.

To illustrate the effects of St and Q on the dynamics of a neutrally buoyant particle, let us consider the simple incompressible two-dimensional model flow defined by the stream function

$$\psi(x, y, t) = A \cos(x + B \sin \omega t) \cos y. \qquad (11)$$

The equations of motion for an element of the fluid will then be $\dot{x} = \partial_y \psi$, $\dot{y} = -\partial_x \psi$. ψ has the rôle of a Hamiltonian for the dynamics of such an element, with x and y playing the parts of the conjugate coordinate and momentum pair. Let us first consider the simplest case, for which we suppress time dependence by setting $B = 0$. Thence ψ should be a constant of motion, which implies that real fluid elements follow trajectories that are level curves of ψ. In Fig. 1(a) are depicted contours of Q. Notice that the high values of Q are around the hyperbolic points, while negative Q coincides with the centres of vortices — elliptic points — in the flow. Figure 1 (top right) shows the trajectory of a neutrally buoyant particle starting from a point on a fluid trajectory within the central vortex,

but with a small velocity mismatch with the flow. This mismatch is amplified in the vicinity of the hyperbolic stagnation points for which Q is larger than $4/9\,\mathrm{St}^{-2}$ to the extent that the particle leaves the central vortex for one of its neighbors, a trip that is not allowed to a fluid parcel. In the end a particle settles on a trajectory that does not visit regions of high Q, proper for a fluid parcel. While this effect is already seen in Fig. 1(b), it is more dramatically pictured in the trajectory shown in Fig. 1(c), in which the particle performs a long and complicated excursion wandering between different vortices before it settles in a region of low Q of one of them. To illustrate the divergence of particle and fluid trajectories, and the fact that particle and fluid finally arrive at an accord, in Fig. 1(d) we display the difference between the particle velocity and the fluid velocity at the site of the particle against time for this case. Notice that this difference seems negligible at time zero, and that it also convergences to zero at long times, but during the interval in which the excursion takes place it fluctuates wildly.

Even more interesting is the case of time-dependent flow: $B \neq 0$ in our model. As in a typical Hamiltonian system, associated with the original hyperbolic stagnation points, there are regions of the phase space — here real space — dominated by chaotic trajectories. Trajectories of this kind, stroboscopically sampled at the frequency of the flow, are reproduced in Fig. 2. Such trajectories visit a large region of the space, which includes the original hyperbolic stagnation points and their vicinities where Q is large. Excluded from the reach of such a chaotic trajectory remain areas where the dynamics is regular; the so-called KAM (Kolmogorov–Arnold–Moser) tori. In our model these lie in the regions where $Q < 4/9\,\mathrm{St}^{-2}$. Now a neutrally buoyant particle trying to follow a chaotic flow pathline would eventually reach the highly hyperbolic regions of the flow. This makes likely its separation and departure from such a pathline, in search of another pathline to which to converge. However, convergence will only be achieved if the pathline never crosses areas of high Q. Figure 2 demonstrates this phenomenon: particles were released in the chaotic zone with a small velocity mismatch. Such a particle follows the flow, until, coming upon a region of sufficiently high Q, it is thrown out of that flow pathline onto a long excursion that finally ends up in a regular region of the flow on a KAM torus. The regular regions of the flow then constitute attractors of the dissipative dynamical system Eq. (10) that describes the behaviour of a neutrally buoyant particle.

IV. DISCRETE DYNAMICS DESCRIPTION

An examination of the dynamical system defining our minimal model for the behavior of neutrally buoyant particles shows that it is composed of some dynamics within some other larger set of dynamics. Eq. (4) can be seen as an equation for a variable that would define another equation of motion, when the solution of the former be zero. Recall that the inner dynamics is that representing the Lagrangian trajectories of the flow, and that in two dimensions, it is a Hamil-
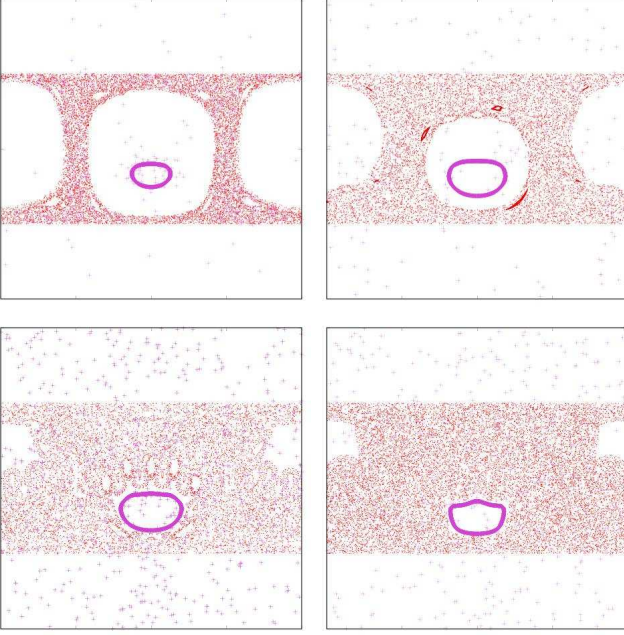
FIG. 2: Poincaré sections of trajectories in the time-dependent flow of Eq. (11). From top left to bottom right are shown (red dots) four increasingly chaotic examples of the flow, and (magenta crosses), the trajectories of neutrally buoyant particles in the flows that in each case finally end up on a KAM torus within the regular region of the flow.

tonian system. We may say that this Hamiltonian system is embedded in a larger dynamical system, this time dissipative, whose trajectories may or may not converge to zero. If they do, the system ends up on the same trajectories as those of the smaller embedded system, but in general this need not be the case. The general concept of some dynamics embedded within some other dynamics may be exploited within the framework of dynamical-systems theory to design techniques that reject some unwanted trajectories of the original dynamics by making them unstable in the embedding, paralleling what the particles do in the fluid-dynamics case. This idea has been dubbed bailout embedding of a dynamical system and has obvious applications to control theory [16].

Trading generality for clarity, in this Section we present an example of a bailout embedding for discrete-time dynamical sytems that closely represents all the qualitative aspects of the above described impurity dynamics. Generally speaking, given a map $\boldsymbol{x}_{n+1} = \boldsymbol{T}(\boldsymbol{x}_n)$ — $\boldsymbol{x}$ being a point in a space of arbitrary dimension — a bailout embedding is the second order recurrence

$$\boldsymbol{x}_{n+2} - \boldsymbol{T}(\boldsymbol{x}_{n+1}) = \mathrm{K}(\boldsymbol{x}_n)(\boldsymbol{x}_{n+1} - \boldsymbol{T}(\boldsymbol{x}_n)), \qquad (12)$$

where $\mathrm{K}(\boldsymbol{x})$ is chosen such that $|\mathrm{K}(\boldsymbol{x})| > 1$ over the unwanted set of orbits, so that they become unstable in the embedding. In the discrete system, almost any expression written for the ordinary differential equation translates to something close to an exponential; in particular, stability eigenvalues have to be

negative in the ordinary-differential-equation case to represent stability, while they have to be smaller than one in absolute value in the map case. In order to simulate the dynamics of particles, the operator $- \left(J + 2/3 \, \mathrm{St}^{-1} \mathrm{I} \right)$ should translate into the particular choice

$$\mathrm{K}(\boldsymbol{x}) = e^{-\gamma} \boldsymbol{\nabla T} \qquad (13)$$

with $\gamma = -2/3 \, \mathrm{St}^{-1}$, in the map setting.

To represent qualitatively a chaotic two-dimensional incompressible base flow we choose a classical testbed of Hamiltonian systems, the area preserving standard map introduced by Taylor and Chirikov:

$$\boldsymbol{T} : (x_n, y_n) \to (x_{n+1}, y_{n+1}), \qquad (14)$$

where

$$\begin{aligned} x_{n+1} &= x_n + \frac{k}{2\pi} \sin(2\pi y_n) \\ y_{n+1} &= y_n + x_{n+1} \end{aligned} \qquad (15)$$

and k is the parameter controlling integrability. Recall that in general, the dynamics defined by this map present a mixture of quasiperiodic motions occurring on the KAM tori and chaotic ones, depending on where we choose the initial conditions. As the value of k is increased, the region dominated by chaotic trajectories pervades more and more of the phase space, except for increasingly small islands of KAM quasiperiodiciy. Hence our qualitative description of the impurity dynamics, the bailout embedding of the standard map, is given by the coupled second-order iterative system defined by Eqs. (12), (13), (14), and (15).

Notice that due to the area-preserving property of the standard map, the two eigenvalues of the derivative matrix must multiply to one. If they are complex, this means that both have an absolute value of one, while if they are real, generically one of them will be larger than one and the other smaller. We can then separate the phase space into elliptic and hyperbolic regions corresponding to each of these two cases. If a trajectory of the original map lies entirely on the elliptic regions, the overall factor $\exp(-\gamma)$ would damp any small perturbation away from it in the embedded system. But for chaotic trajectories that inevitably visit some hyperbolic regions, there exists a value of γ such that perturbations away from a standard-map trajectory are amplified instead of dying out in the embedding. As a consequence, trajectories are expelled from the chaotic regions finally to settle in the elliptic KAM islands.

To illustrate this, Fig. 3 shows the phenomenon in a situation in which the nonlinearity parameter has been set to the value $k = 7$. This corresponds to a very chaotic region of the standard map, characterized by the existence of minute KAM islands within a sea of chaos that covers almost all the available phase space. Fig. 3(a) is a close-up — to make it visible — of the largest of these islands and the dots there represent the successive positions of a set of 1000 fluid parcels — evolving according to the standard map — spread initially at random over the unit cell. Since none of these parcels were initially located inside the island, this is seen as a white spot
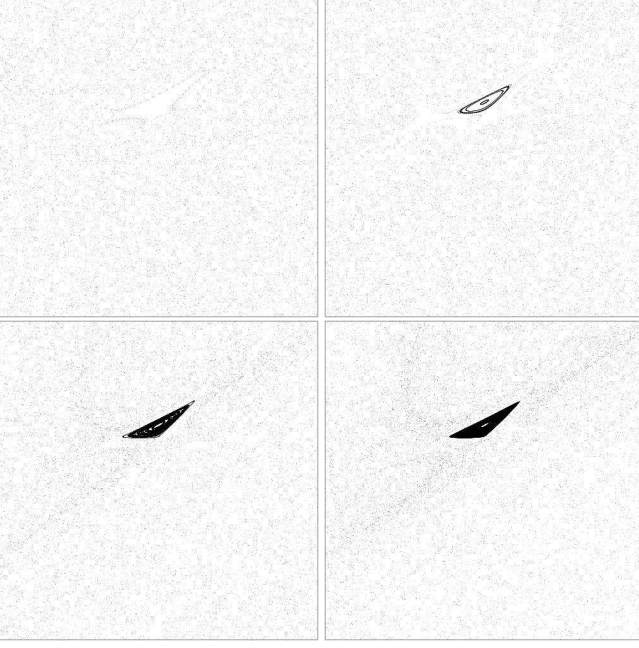
FIG. 3: The standard map for $k = 7$ has a chaotic sea covering almost the entire torus, except for a tiny period-two KAM island near position $0, 2/3$. 1000 random initial conditions were chosen, iterated for 20000 steps, then the next 1000 iterations are shown. The images here are a box $-0.05 < x < 0.05$, $0.61 < p < 0.71$. (a) Original map, (b) $\gamma = 1.4$, (c) $\gamma = 1.3$, (d) $\gamma = 1.2$.

never visited by the parcels. In contrast, in Figs 3(b), 3(c), and 3(d), the dots are the successive positions, after a number of equilibration iterations, of particles initially placed as the parcels in Fig. 3(a), but allowing a very small initial discrepancy $\boldsymbol{\delta}_0 = \boldsymbol{x}_1 - \boldsymbol{T}(\boldsymbol{x}_0)$ of both dynamics. Notice that now, although having started initially outside the island, some of the particles settle inside in a process that becomes increasingly marked as the parameter γ decreases.

V. NOISY DYNAMICS

By virtue of volume preservation, the invariant measure of the fluid-parcel dynamics is either uniform, if the system is ergodic, or else disintegrates into a foliation of KAM tori and ergodic regions, otherwise. In any case, the addition of a small amount of white noise, which may be considered to represent the effects of small scale turbulence, thermal fluctuations, etc., renders the system ergodic with only a uniform invariant measure. Thus, the distribution of fluid particles is expected to be uniform with or without the presence of noise. The situation is however very different if the noise is applied to the dynamics of the particles, or, correspondingly, to the bailout embedding.

Let us consider the following stochastic discrete-time dynamics

$$
\begin{aligned}
\boldsymbol{x}_{n+2} - \boldsymbol{T}(\boldsymbol{x}_{n+1}) &= e^{-\gamma} \boldsymbol{\nabla T}|_{\boldsymbol{x}_n} (\boldsymbol{x}_{n+1} - \boldsymbol{T}(\boldsymbol{x}_n)) \\
&\quad + \boldsymbol{\xi}_n,
\end{aligned}
\tag{16}
$$

in which, as in the previous Section, $\boldsymbol{x}$ represents the particle coordinates and $\boldsymbol{T}(\boldsymbol{x})$ the fluid parcel evolution. New here is the noise term ξ_n, with statistics

$$
\begin{aligned}
\langle \boldsymbol{\xi}_n \rangle &= 0, \\
\langle \boldsymbol{\xi}_n \boldsymbol{\xi}_m \rangle &= \varepsilon (1 - e^{-2\gamma}) \, \delta_{m.n} \, \mathrm{I}.
\end{aligned}
\tag{17}
$$

This term forces the particle away from the fluid trajectory at every step of the dynamics. However, the actual magnitude of the fluctuations induced in $\boldsymbol{x}$ will be modulated by the properties of $\boldsymbol{\nabla T}$ — the flow gradients — along the particle trajectory. Notice that for practical reasons we vary the noise intensity in correspondence with γ in order to obtain comparable fluctuations at different values of this parameter.

Let us again consider the standard map as modelling the basic flow, and its noisy bailout embedding that represents a particulate impurity subject to both fluid drag and noise forces. We are interested in the asymptotic stationary behavior of an ensemble of such particles which, invoking the ergodicity of the fluctuations, should be well represented by the the histogram of visits that a single particle pays to each bin of the space — the full phase space for the basic flow, but a projection of the full phase space for the particles — as time goes by.

Figure 4 displays a sequence of these histograms in a scaled color code for the same nonlinearity parameter $k = 7$ as in Fig. 3, corresponding to the extremely chaotic regime of the standard map considered in the previous Section. The sequence of images corresponds to increasing the stability parameter $\exp(-\gamma)$. The images make evident the fine filamentary structure developed by the asymptotically invariant distributions due to the combined effect of noise and the ability of particles to separate from the basic flow. Remarkably, however, these structures appear even in the case in which the γ values are larger than those required to produce a spontaneous detachment of the particle trajectories.

Notice that the filamentation here arises from the existence of avenues in the phase space that lead to the small KAM islands on which the particles prefer to stay. A more detailed analysis shows that on these avenues the average value of the squared separation between particles and fluid trajectories is relatively small. Roughly parallel to these avenues, on the other hand, there are strips of the phase space that the particles avoid. There, the separation between particle and fluid trajectories is on average much larger. Filamentation is thus due to the tendency of the particles to avoid neighboring regions.

The same mechanism may also lead to patchiness, not necessarily filamentary. Looking at flows with weaker chaos, for example, for which relatively large KAM islands coexist with comparably sized regions of chaos, a situation such as the one shown in Fig. 5 is typical. There there are relatively small avoided regions that separate large patches of larger concentration of particles around the nonchaotic islands. This picture is also testimonial to a property that distinguishes the present mechanism from those of Refs. [4, 5]. While there the particles group around the unstable manifolds of the homoclinic intersections of the basic flows, in our case instead the impurity dynamics tend to avoid the invariant manifolds. This is
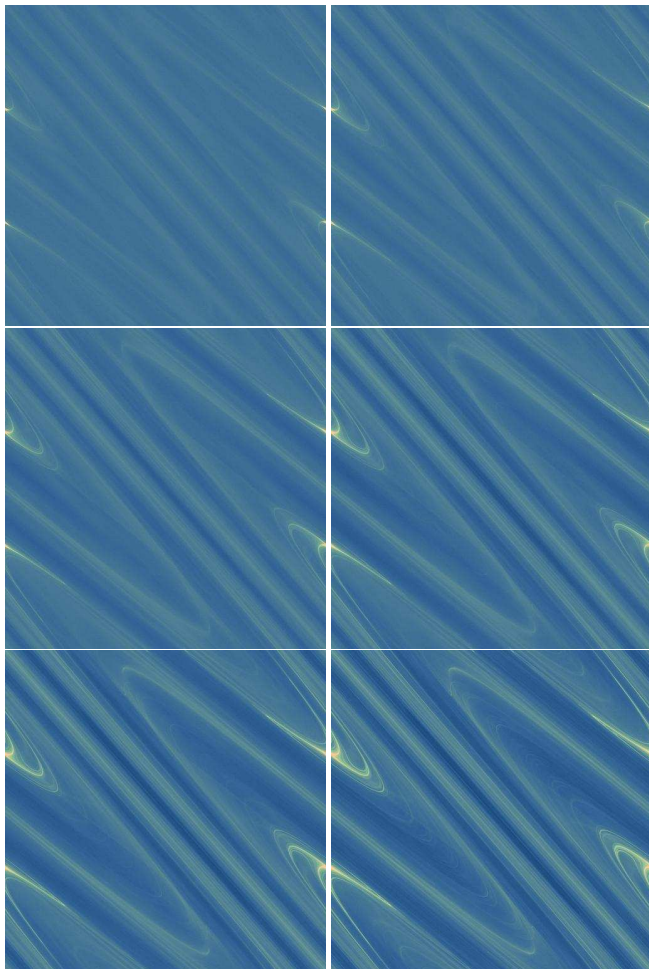
FIG. 4: Histograms with intensity encoding as the square root of invariant probability. Parameters are standard map parameter $k = 7.0$, $\varepsilon = 10^{-9}$, and, from top left to bottom right, stability parameter $\gamma = 0.5, 0.6, 0.7, 0.8, 0.9$, and 1.0.

FIG. 5: Histogram with standard map parameter $k = 2.0$, $\varepsilon = 10^{-7}$, and stability parameter $\gamma = 0.8$.

because following these manifolds would mean hitting eventually regions in which the Jacobian eigenvalues are closer to one, which locally amplifies the effect of fluctuations on the dynamics of the particles.

VI. DISCUSSION AND CONCLUSIONS

It has previously been demonstrated that small neutrally buoyant particles immersed in a fluid flow, and therefore subject to drag forces, may follow trajectories that spontaneously separate from those of the fluid parcels in some regions of the flow. Specifically, this occurs when the shear is very strong compared to the Stokes number associated with the particles. Given that in general, the smaller the particles are, the stronger is the shear necessary for this phenomenon to manifest itself, the actual condition for separation may not be fulfilled by some fluid flows of physical interest. However, we hav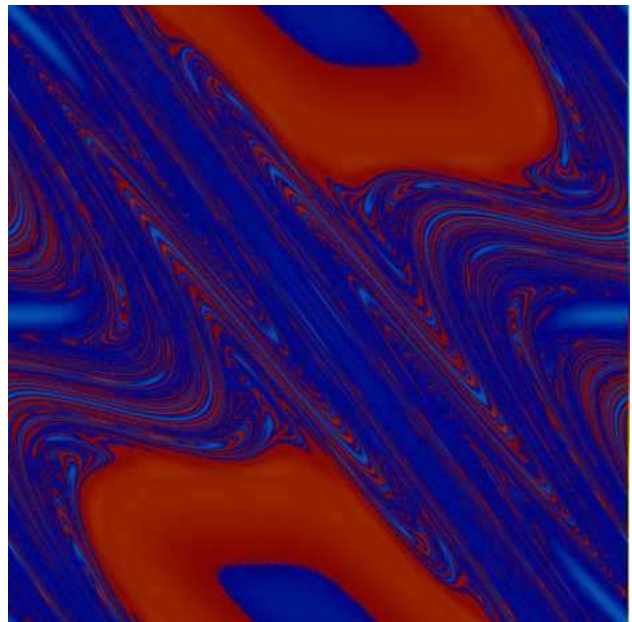e shown here that the addition of noise to the forces acting on the particles may extend the consequences of this phenomenon beyond the range of Stokes numbers for which separation is possible in an interesting way, namely, the generation of inhomogeneities in the asymptotic distributions of these particles even in cases where the flow is a highly efficient mixer.

There is a large variety of examples in which noise ought naturally to be added to the dynamical equations of the particles. Thermal fluctuations, for example should be considered in a range of small-scale laboratory experiments. The effect of small-scale turbulence forcing drifters in oceanographic applications might also be another relevant example. In the case of plankton dynamics, in which the arisal of inhomogeneous distributions is an issue, the autonomous swimming abilities of individuals might be viewed as an internal source of noise. But could the phenomenon described here be the basis of the plankton distribution patchiness? If each individual plankton is naively considered as an impurity particle, the answer is obviously not: their size is far too small for these effects to be appreciable. But if there are grounds to consider plankton in large-scale colonies moving more or less rigidly in the ocean, the consequences of the phenomenon described here need to be taken seriously.

We conclude with an epistemological note: the dynamics of neutral particles in flows has suggested to us a generalization to maps that helps to solve some problems in the general domain of Hamiltonian dynamics. This generalization in turn pays us back by suggesting a way in which inhomogeneous distributions may arise in fluid-dynamical problems. We believe that this is a remarkable instance OF mutual convenience in the interdisciplinary marriage between the two fields.

[1] E. R. Abraham, Nature **391**, 577 (1998).

[2] S. A. Levin and L. A. Segal, Nature **259**, 659 (1976).

[3] *Spatial Patterns in Plankton Communities*, edited by H. J. Steele (Plenum, 1978).

[4] C. Jung, T. Tél, and E. Ziemniak, Chaos **3**, 555 (1993).

[5] Z. Toroczkai *et al.*, Phys. Rev. Lett. **80**, 500 (1998).

[6] Z. Neufeld, C. López, and P. H. Haynes, Phys. Rev. Lett. **82**, 2606 (1999).

[7] A. Babiano, J. H. E. Cartwright, O. Piro, and A. Provenzale, in *Coherent Structures in Complex Systems*, Vol. 567 of *Lecture Notes in Physics*, edited by D. Reguera, L. Bonilla, and M. Rubi (Springer, 2001), pp. 114–126.

[8] A. Babiano, J. H. E. Cartwright, O. Piro, and A. Provenzale, Phys. Rev. Lett. **84**, 5764 (2000).

[9] M. Feingold, L. P. Kadanoff, and O. Piro, J. Stat. Phys. **50**, 529 (1988).

[10] O. Piro and M. Feingold, Phys. Rev. Lett. **61**, 1799 (1988).

[11] J. H. E. Cartwright, M. Feingold, and O. Piro, Physica D **76**, 22 (1994).

[12] J. H. E. Cartwright, M. Feingold, and O. Piro, J. Fluid Mech. **316**, 259 (1996).

[13] J. H. E. Cartwright, M. Feingold, and O. Piro, Phys. Rev. Lett. **75**, 3669 (1995).

[14] M. Abel, A. Celani, D. Vergni, and A. Vulpiani, Phys. Rev. E **64**, 046307 (2001).

[15] C. López *et al.*, Chaos **11**, 397 (2001).

[16] J. H. E. Cartwright, M. O. Magnasco, and O. Piro, submitted (2001).

[17] M. R. Maxey and J. J. Riley, Phys. Fluids **26**, 883 (1983).

[18] E. E. Michaelides, J. Fluids Eng. **119**, 233 (1997).

[19] G. I. Taylor, Proc. Roy. Soc. Lond. A **120**, 260 (1928).

[20] T. R. Auton, J. C. R. Hunt, and M. Prud'homme, J. Fluid Mech. **197**, 241 (1988).

[21] J. Boussinesq, C. R. Acad. Sci. Paris **100**, 935 (1885).

[22] A. B. Basset, Phil. Trans. Roy. Soc. Lond. **179**, 43 (1888).

[23] H. Faxén, Ann. Phys. **4**, 89 (1922).

[24] A. Okubo, Deep-Sea Res. **17**, 445 (1970).

[25] J. B. Weiss, Physica D **48**, 273 (1991).